Supporting Information

Revealing Failure Mechanism of Transition-Metal Chalcogenides towards Copper Current Collector in Secondary Batteries

Guannan Zu[a], Gencai Guo[a], Hongyi Li*[a], Yue Lu[b], Ruzhi Wang[a], Yuxiang Hu[c], Lianzhou Wang*[c] and Jinshu Wang*[a]

[a] *Key Laboratory of Advanced Functional Materials of Education Ministry of China, College of Materials Science and Engineering, Beijing University of Technology, Beijing, 100124, China. Email: lhy06@bjut.edu.cn, wangjsh@bjut.edu.cn. Tel.: +86-67391101*

[b] *Institute of Microstructure and Properties of Advanced Materials, Beijing University of Technology, Beijing, 100124, China.*

[c] *Nanomaterials Centre, Australian Institute for Bioengineering and Nanotechnology, and School of Chemical Engineering, The University of Queensland, Australia. Email: l.wang@uq.edu.au*

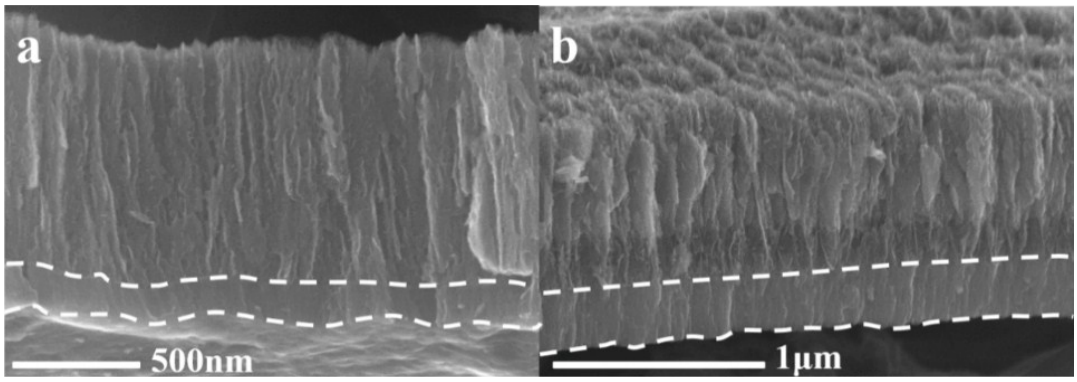

Fig. S1 SEM cross section view of (a) Cu/1hTi/MoS_2, (b) Cu/2hTi/MoS_2 (the white lines in (a) and (b) illustrated sputtered Ti layers).

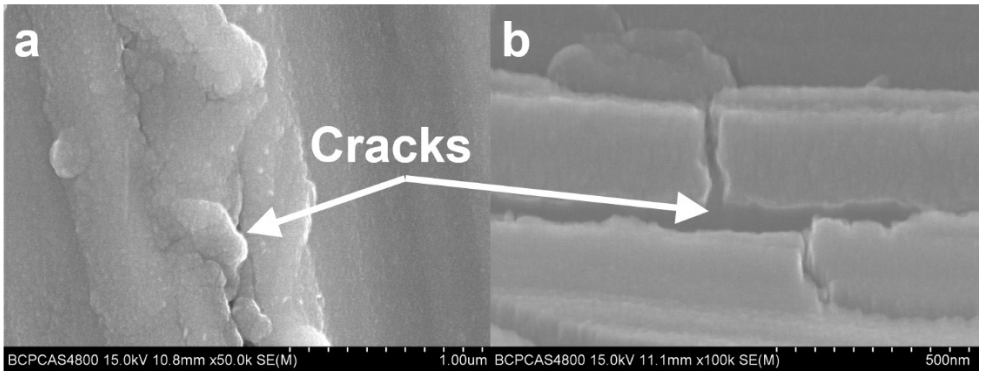

Fig. S2 (a) SEM image and (b) cross section view of Cu/1hTi.

Table S1 Representative experiments on TMCs in secondary batteries.

Control groups	Conclusion
(a) $Cu_{thin\ foil}/MoS_2$ and $Cu_{thin\ foil}$/2hTi/MoS_2	The traditional Cu thin foils could also arise the generation of Cu_2S NPs.
(b) Cu/MoS_2 and Cu/2hW/MoS_2	Ti was not the only choice for the construction of passivation layer between Cu and MoS_2
(c) Cu/MoS_2 and Cu/C/MoS_2	Ti was not the only choice for the construction of protection layer between Cu and MoS_2
(d) Cu/MoS_2 (prepared at 25 °C)	The formation of Cu_2S wasn't related to the preparation temperature.
(e) Cu/2hCu/MoS_2	The influence of CuO (might generate during polishing) was validated, we found that the generation of Cu_2S wasn't related to CuO.
(f) Ti/MoS_2	The cycling performance was similar with that of Cu/Ti/MoS_2.
(g) Cu/WS_2 and Cu/2hTi/WS_2	WS_2 showed the same failure mechanism with MoS_2. The improvement strategy was effective for WS_2.
(h) Cu/FeS and Cu/2hTi/FeS	FeS showed the same failure mechanism with FeS. The improvement strategy was effective for FeS.
(i) $Cu_{thin\ foil}/MoS_{2\ bulk\ powder}$	Based on the conventional slurry/coating method, Cu_2S could be observed in $Cu_{thin\ foil}/MoS_{2\ bulk\ powder}$ resultant prepared by the conventional slurry/coating method

[a] All the metal layers (Ti, W, Cu) have been prepared for 2 h, with direct current power of 200 W at 400 °C. All the TMCs films have been prepared for 1 h, with radio frequency power of 100 W at 400 °C.

[b] Cu foil-Φ16 mm, 0.5 mm in thickness, 99.95% in purity, $Cu_{thin\ foil}$-Φ16 mm, 9 μm in thickness.

[c] The batteries in Table S1 were tested at the current density of 1 C with the window of 0.1-3 V at room temperature.

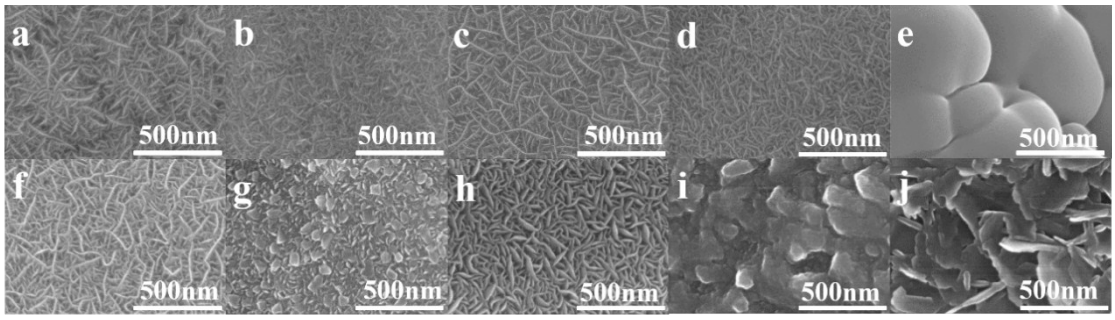

Fig. S3 SEM images of (a) $Cu_{thin\ foil}/MoS_2$, (b) $Cu_{thin\ foil}$/2hTi/MoS_2, (c) Cu/2hW/MoS_2, (d) Cu/MoS_2 (prepared at room temperature), (e) Cu/2hCu/MoS_2, (f) Ti/MoS_2, (g) Cu/WS_2, (h) Cu/2hTi/WS_2, (i) Cu/FeS, (j) Cu/2hTi/FeS.

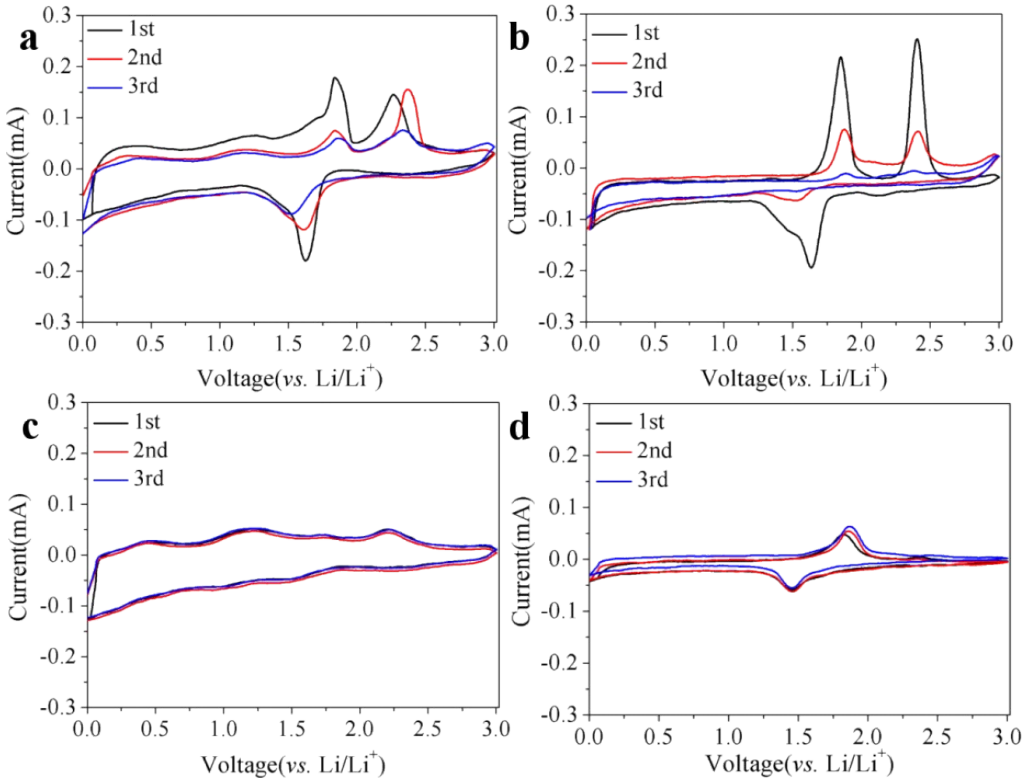

Fig. S4 CV curves of (a) Cu/WS_2 and (c) Cu/2hTi/WS_2, (b) Cu/FeS and (d) Cu/2hTi/FeS. The CV curves were obtained at the scan rate of 0.1 mVs^{-1} and sweep window of 0-3 V.

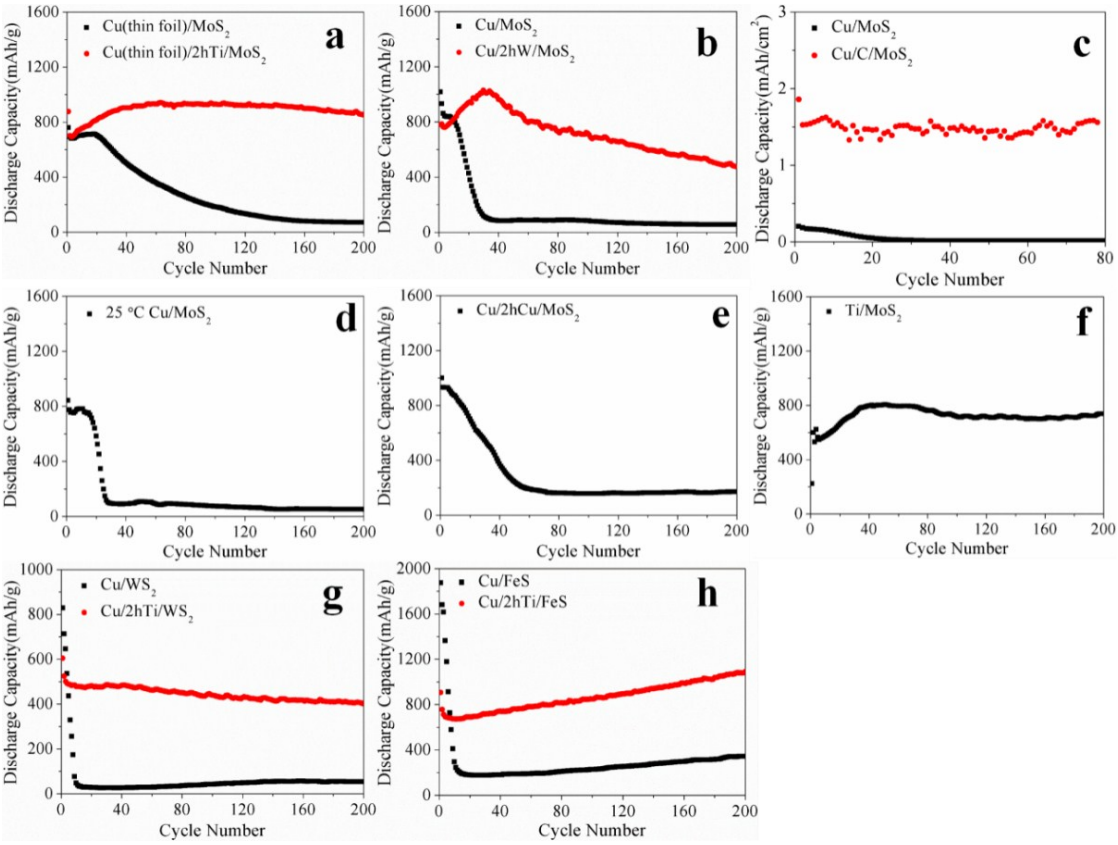

Fig. S5 Cycling performance of different samples corresponding to Table S1.

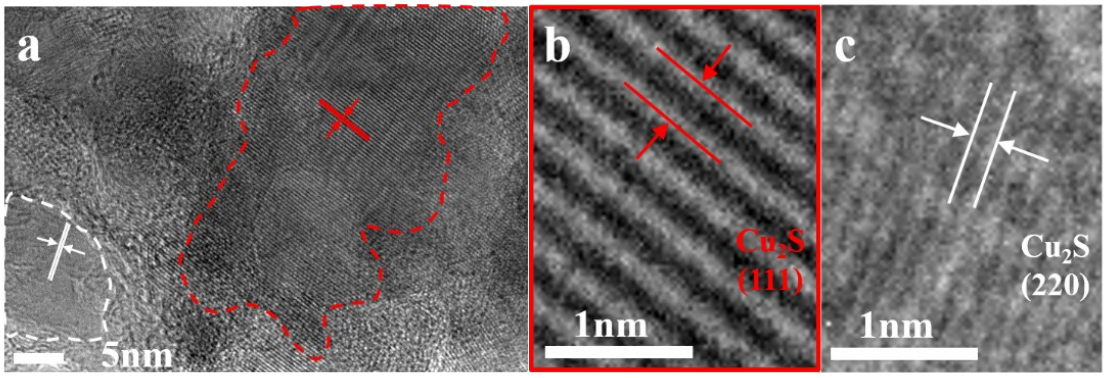

Fig. S6 TEM images of the other Cu/MoS_2 sample after 200-cycle test at 1 C. (a) low magnitude, (b) enlarged image of the red line area in (a), (c) enlarged image of the white line area in (a).

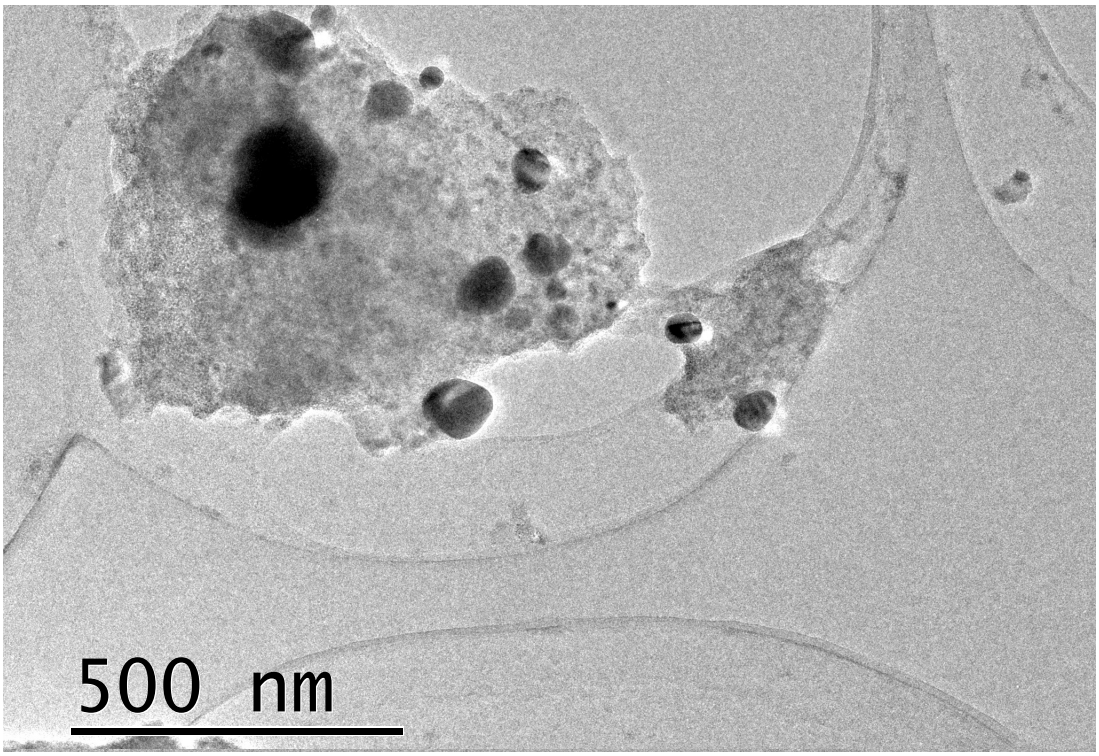

Fig. S7 TEM image of Cu/MoS_2 anode after cycling.

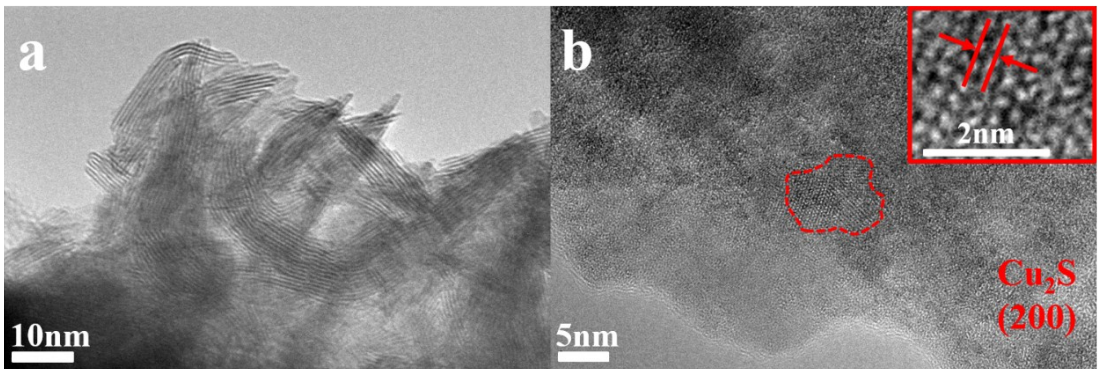

Fig. S8 TEM images of Cu/MoS_2 (prepared at 25 °C) anode in LIBs (a) before and (b) after cycling at 1 C. The inset image was the enlarged figure of the red area in (b).

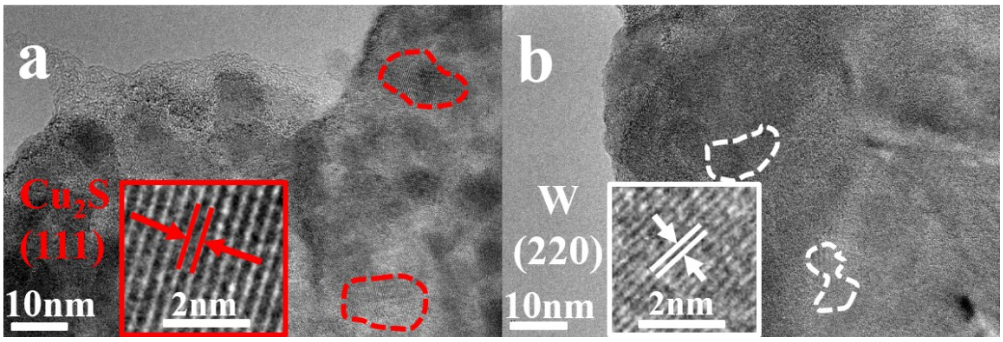

Fig. S9 TEM images of (a) Cu/WS_2 and (b) Cu/2hTi/WS_2 anode in LIBs after cycling at 1 C.

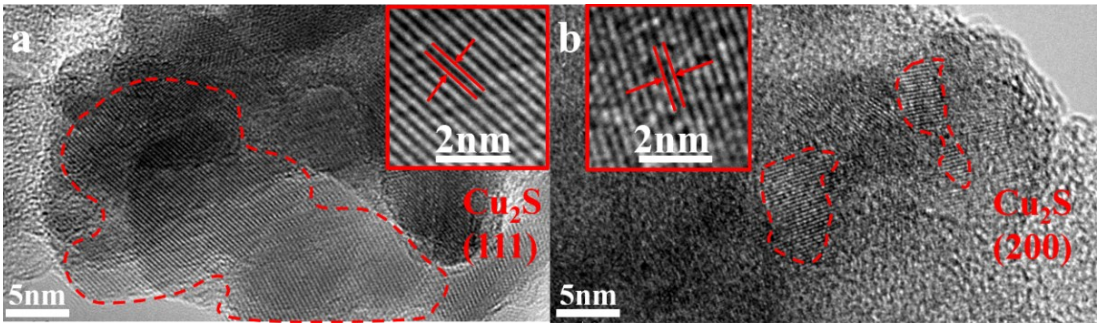

Fig. S10 TEM images of (a) Cu/FeS and (b) Cu/2hTi/FeS anode in LIBs after cycling at 1 C.

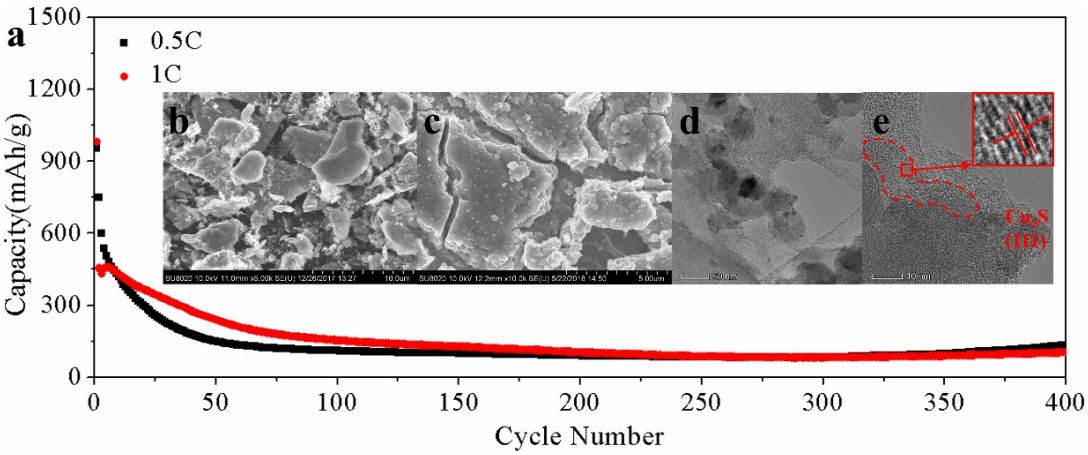

Fig. S11 (a) The cycling performance of commercial bulk MoS_2 powder at 0.5 and 1 C, SEM images of the mixture of MoS_2 powder, carbon black and PVDF (b) before cycling, (c) after cycling, TEM images of MoS_2 after cycling (d) low magnitude, (e) high resolution. The inset TEM image in Fig. S12e was the enlarged figure of the red line area.

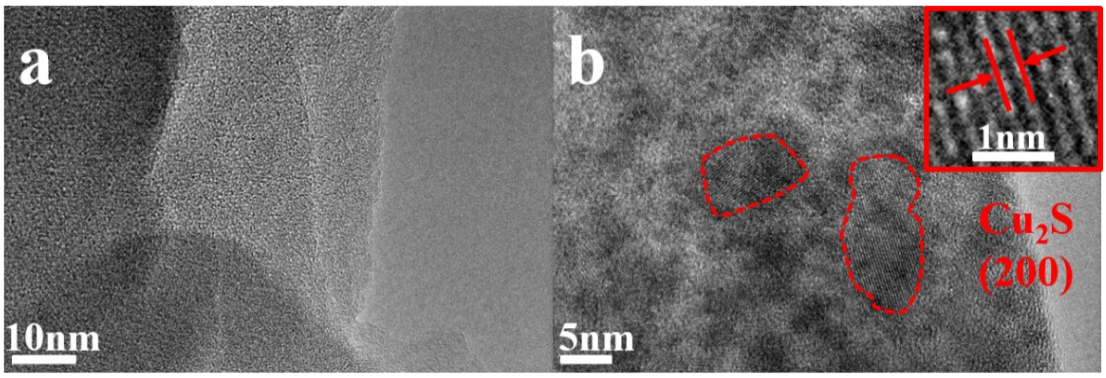

Fig. S12 TEM images of Cu/2hCu/MoS_2 anode in LIBs (a) before and (b) after cycling at 1 C.

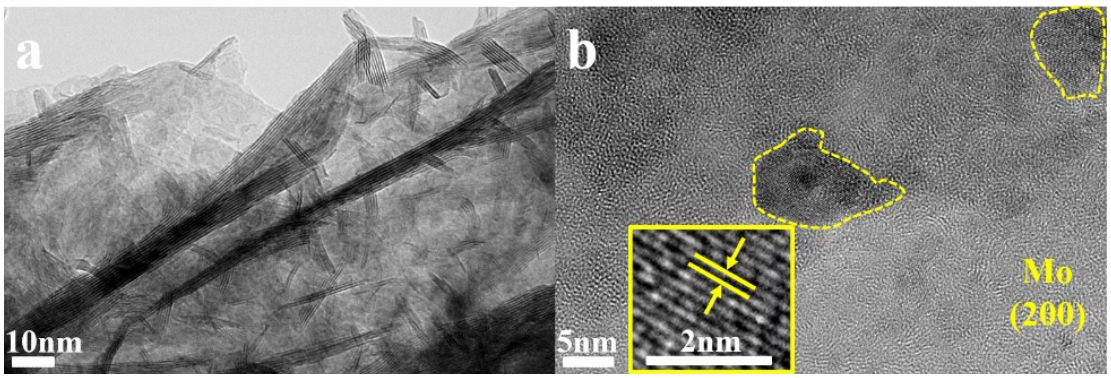

Fig. S13 TEM images of Ti/MoS_2 anode in LIBs (a) before and (b) after cycling at 1 C.

Table S2 Formation energy of different substances according to the first-principles calculations

Structure	**E (eV/formula)**
MoS_2 (bulk)	-21.7940059
Cu (metal)	-3.72875892
Cu_2S (bulk)	-11.74212656
Li (bulk)	-1.898217485
Li_2S (bulk)	-11.96849764
Mo (metal)	-10.94908539
S(bulk)	-4.12142378562
S_8(bulk, single atom)	-4.12329825219

(Eq. S1) $2Cu+Li_2S \rightarrow Cu_2S+2Li$ ΔH= 3.89eV Endothermic reaction
(Eq. S2) $4Cu+MoS_2 \rightarrow 2Cu_2S+Mo$ ΔH= 2.28 eV Endothermic reaction
(Eq. S3) $2Cu+S \rightarrow Cu_2S$ ΔH= -0.16 eV Exothermic reaction
(Eq. S4) $16Cu+S_8 \rightarrow 8Cu_2S$ ΔH= -1.29 eV Exothermic reaction

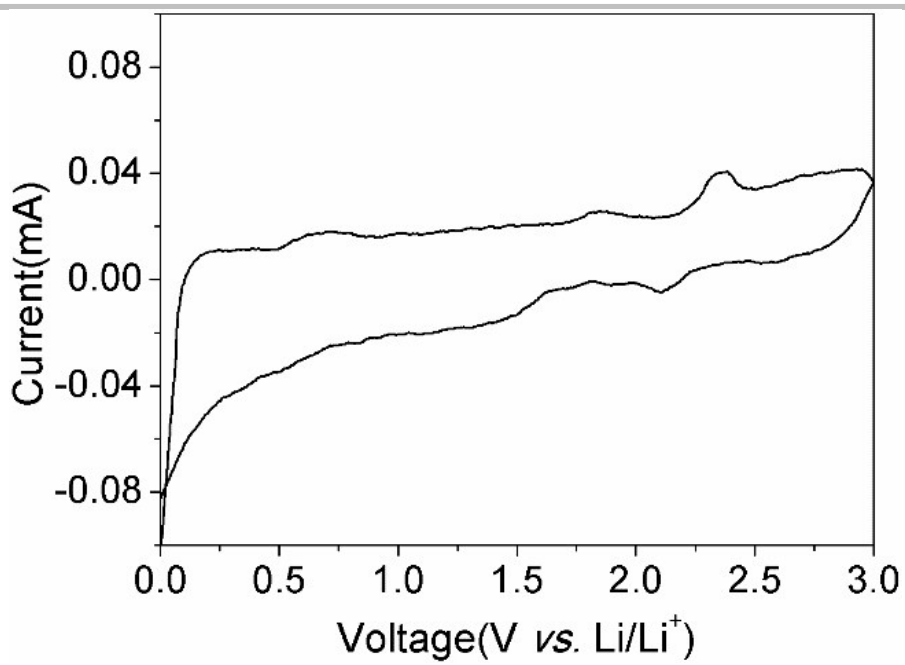

Fig. S14 CV curve of Cu/MoS_2 after 30 cycles tested at 1 C.

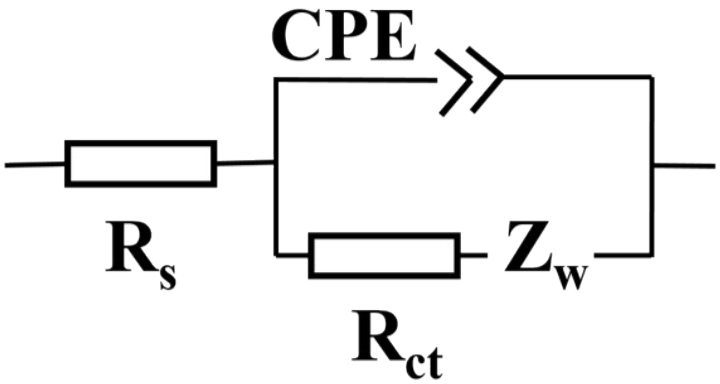

Fig. S15 Simulated circuit of the EIS test.

Experimental section of MoS_2 in SIBs

The preparation procedures of Cu/MoS_2 and Cu/2hTi/MoS_2 have been described in the main manuscript. The SIBs adopted Na metal as the counter electrode and 1 M $NaClO_4$ dissolved in propylene carbonate/fluoroethylene carbonate (PC: 2% FEC) as the electrolyte. Glass fiber (GF/A: 1.6 μm, Whatman, America) acted as the separator. The galvanostatic charge and discharge measurements were carried out on CT2001A model (LANHE, China) with the testing window of 0.1-3 V (vs. Na/Na^+) at different current densities at room temperature. Cyclic voltammograms (CV) measurement was performed on a ParSTAT MC electrochemical working station (Ametek Advanced Measurement Technology, America) with the window of 0-3 V. The samples were used as anodes to assemble 2032-coin cells in an argon-filled glove box with both H_2O and O_2 concentration below 0.5 ppm.

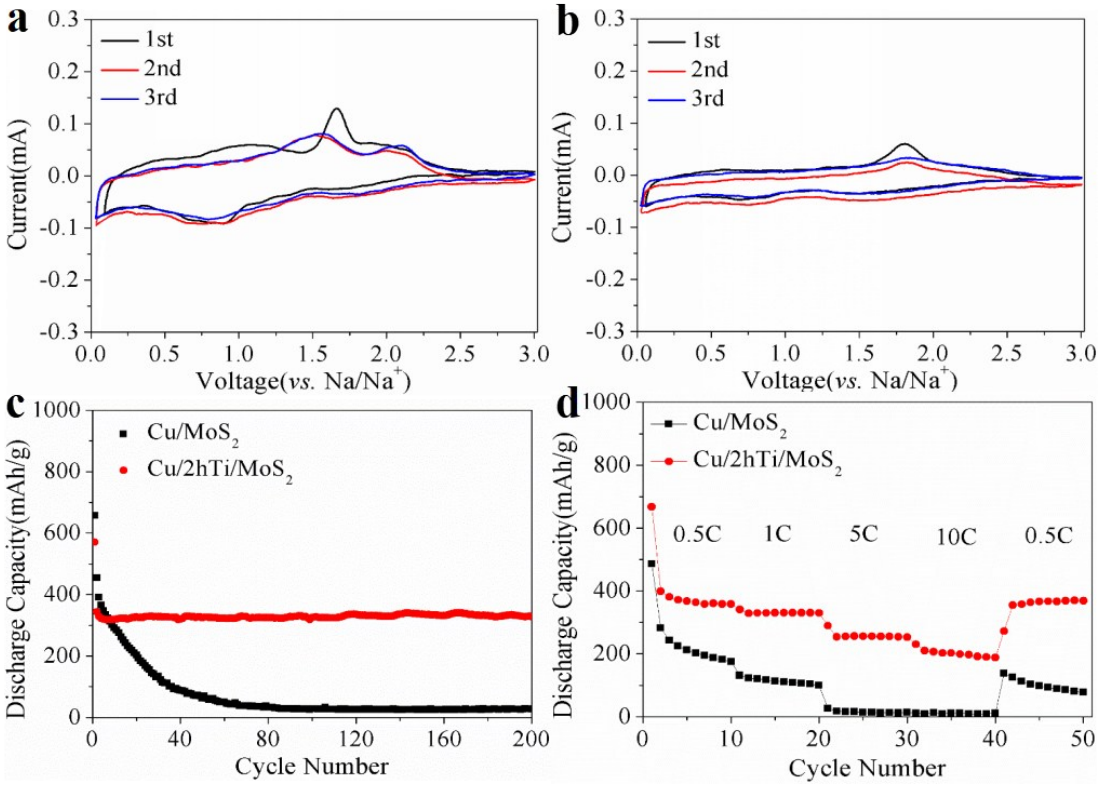

Fig. S16 CV curves of (a) Cu/MoS_2 and (b) Cu/2hTi/MoS_2 in SIBs, (c) cycling test and (d) rate performance of Cu/MoS_2 and Cu/2hTi/MoS_2.

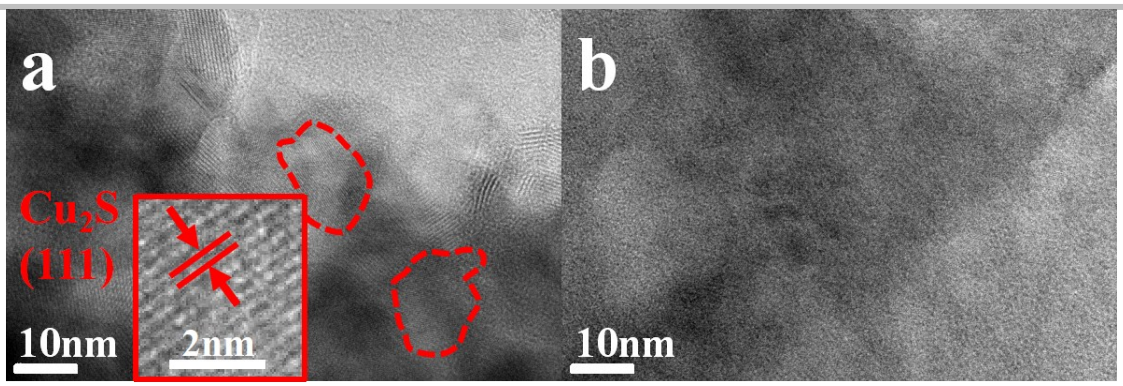

Fig. S17 TEM images of (a) Cu/MoS_2 and (b) Cu/2hTi/MoS_2 anodes in SIBs after cycling at 1 C.

After disassembling the cycled SIBs, TEM characterization was carried out, as shown in Figure S16. Cu_2S NPs were observed on Cu/MoS_2 resultant (Figure S17a), while none was observed in the cycled Cu/2hTi/MoS_2 resultant (Figure S17b). This result indicated that the corrosive side reaction between Cu and S also occurred in TMCs-based anode in SIBs, which was the other convincing evidence of the corrosion mechanism in rechargeable batteries.